EBioMedicine 20 (2017) 230–239

Contents lists available at ScienceDirect

EBioMedicine

journal homepage: www.ebiomedicine.com

Research Paper

Disruption of the Hepcidin/Ferroportin Regulatory System Causes Pulmonary Iron Overload and Restrictive Lung Disease

Joana Neves [a,b,c,d], Dominik Leitz [d,e], Simone Kraut [f], Christina Brandenberger [g], Raman Agrawal [d,e], Norbert Weissmann [f], Christian Mühlfeld [g], Marcus A. Mall [b,d,e,1], Sandro Altamura [a,b,1], Martina U. Muckenthaler [a,b,d,*,1]

[a] Department of Pediatric Hematology, Oncology and Immunology - University of Heidelberg, Im Neuenheimer Feld 350, D-69120 Heidelberg, Germany
[b] Molecular Medicine Partnership Unit, D-69120 Heidelberg, Germany
[c] Graduate Program in Areas of Basic and Applied Biology, Abel Salazar Biomedical Sciences Institute, University of Porto, 4050-343 Porto, Portugal
[d] Translational Lung Research Center Heidelberg (TLRC), German Center for Lung Research (DZL), University of Heidelberg, D-69120 Heidelberg, Germany
[e] Department of Translational Pulmonology, University of Heidelberg, D-69120 Heidelberg, Germany
[f] Justus-Liebig University of Giessen (JLUG), Excellence Cluster Cardiopulmonary System (ECCPS), Universities of Giessen and Marburg Lung Center (UGMLC), German Center for Lung Research (DZL), Germany
[g] Institute of Functional and Applied Anatomy, Biomedical Research in Endstage and Obstructive Lung Disease Hannover (BREATH), German Center for Lung Research (DZL), Hannover Medical School, D-30625 Hannover, Germany

ARTICLE INFO

Article history:
Received 19 January 2017
Received in revised form 27 April 2017
Accepted 28 April 2017
Available online 29 April 2017

Keywords:
Restrictive lung disease
Ferroportin
Hereditary hemochromatosis
Iron Overload
Hepcidin resistance

ABSTRACT

Emerging evidence suggests that pulmonary iron accumulation is implicated in a spectrum of chronic lung diseases. However, the mechanism(s) involved in pulmonary iron deposition and its role in the in vivo pathogenesis of lung diseases remains unknown. Here we show that a point mutation in the murine ferroportin gene, which causes hereditary hemochromatosis type 4 ($Slc40a1^{C326S}$), increases iron levels in alveolar macrophages, epithelial cells lining the conducting airways and lung parenchyma, and in vascular smooth muscle cells. Pulmonary iron overload is associated with oxidative stress, restrictive lung disease with decreased total lung capacity and reduced blood oxygen saturation in homozygous $Slc40a1^{C326S/C326S}$ mice compared to wild-type controls. These findings implicate iron in lung pathology, which is so far not considered a classical iron-related disorder.

1. Introduction

Imbalances of iron homeostasis are implicated in a spectrum of acute and chronic lung diseases (Ghio, 2009; Ghio et al., 2013). In patients with chronic obstructive pulmonary disease (COPD), iron deposits in alveolar macrophages (AM) and the percentage of iron loaded macrophages is associated with increased disease severity (Philippot et al., 2014). On the other hand thalassemia major, a disease characterized by transfusional iron overload, has been associated with impaired lung function (Carnelli et al., 2003; Guidotti et al., 2016; Kanj et al., 2000). However, whether pulmonary iron accumulation contributes to disease onset and progression is poorly understood.

Tissue iron levels must be maintained in such a way that both iron deficiency and iron overload are prevented. Excess free iron generates oxidative stress causing cell damage and tissue injury (Muckenthaler et al., 2017). In the lung, the risk for oxidative stress is exacerbated by its continuous exposure to an atmosphere with high oxygen levels. The mechanisms maintaining lung iron homeostasis are incompletely understood. Like most other cells, lung cells acquire transferrin-bound iron from the plasma. In addition, lung airway epithelial cells take up iron via the divalent metal transporter 1 (DMT1) and sequester it in the iron storage protein ferritin (Ghio, 2009; Wang et al., 2002). Upon iron exposure, pulmonary ferritin levels increase, possibly protecting from oxidative stress (Ghio, 2009; Ghio et al., 1998; Giorgi et al., 2015).

The supply of iron to the lung depends on its systemic plasma availability, which is controlled by the hepcidin/ferroportin regulatory axis (Muckenthaler et al., 2017). Hepatic hepcidin produced in response to increased systemic iron levels binds to the iron exporter ferroportin (FPN) to control its internalization, ubiquitination and subsequent lysosomal degradation (Nemeth et al., 2004; Qiao et al., 2012). In turn, this decreases iron efflux from exporting cells, such as duodenal enterocytes and reticuloendothelial macrophages. Mutations in the iron exporter FPN that confer resistance to hepcidin binding cause hereditary hemochromatosis (HH) type 4, a genetically inherited

* Corresponding author.
E-mail address: martina.muckenthaler@med.uni-heidelberg.de (M.U. Muckenthaler).
[1] Equal contribution.

http://dx.doi.org/10.1016/j.ebiom.2017.04.036

primary iron overload disorder hallmarked by increased systemic iron levels, iron depletion in iron-exporting organs and severe iron deposition in parenchymal tissues (Altamura et al., 2014; Sham et al., 2009; Sham et al., 2005).

Here, we aim to understand whether a disruption in the FPN/hepcidin regulatory system and the subsequent increase in systemic iron levels affect lung iron homeostasis and function. To achieve this goal, we took advantage of a murine disease model of HH type 4, hallmarked by a C326S amino acid substitution in FPN ($Slc40a1^{C326S}$) (Altamura et al., 2014). We show that resistance of ferroportin to hepcidin binding causes pulmonary iron accumulation in defined lung cell types. Homozygous $Slc40a1^{C326S/C326S}$ mice show increased oxidative stress in the lung, restrictive lung disease and decreased blood oxygen saturation, revealing a role of iron in lung pathology.

2. Material and Methods

2.1. Mice

All mice analyzed were maintained on a pure C57BL/6N genetic background (>99.9% congenic). As controls, age- and gender-matched wild-type C57BL/6N mice born and maintained in the same breeding facility were used. Mice were housed in the Heidelberg University animal facility under a constant light-dark cycle and maintained on a standard mouse diet (LASQCdiet Rod18-A - LASvendi) containing 200 ppm iron with ad libitum access to food and water. All mouse breeding and animal experiments were approved by the Regierungspräsidium Karlsruhe (Projects Nr T-81/14, T-66/13, G-41/16, G-39/16).

2.2. Tissue Iron Quantification

Tissue non-heme iron content was measured using the bathophenanthroline method and calculated against dry weight tissue (Torrance and Bothwell, 1968).

2.3. RNA Extraction, Reverse Transcription and qRT-PCR

Total lung RNA was isolated using Trizol (Life technologies) and was reverse transcribed and used in SYBR-green qPCR, as described in (Altamura et al., 2010). mRNA expression was calculated relative to RPL19 and data were analyzed using the ΔΔCt method (Livak and Schmittgen, 2001). The primers used are listed in Supplementary Information.

2.4. Western Blotting

Protein lysates were obtained by homogenizing snap-frozen tissues in RIPA buffer supplemented with protease inhibitors (Roche Diagnostics), as described in (Galy et al., 2004). Protein concentration was determined using the DC protein assay (BioRad). 50 μg of protein were subjected to western-blot analysis with the antibodies listed in Supplementary Information. Western blot images were quantitatively acquired with the Vilber Lourmat Fusion-FX Chemiluminescence system (Eberhardzell). β-actin was used as loading control.

2.5. Lipid Peroxidation - TBARS Measurements

Thiobarbituric acid reactive substances (TBARS) levels were measured in samples of total lung from 36-week old mice using the QuantiChrom TBARS Assay Kit (BioAssay Systems) following manufacturer's instructions.

2.6. Bronchoalveolar Lavage and Differential Cell Count

Mice were anesthetized via intraperitoneal injection of a combination of ketamine and xylazine (120 and 16 mg/kg respectively) and sacrificed by exsanguination. A median sternotomy was performed, the trachea cannulated and the left mainstem bronchus ligated, and the right lung was lavaged with Phosphate Buffered Saline (PBS). Bronchoalveolar lavage (BAL) samples were centrifuged and BAL fluid supernatant was harvested and stored at −80 °C. Total cell counts were determined using a haemocytometer and differential cell counts were determined in cytospin preparations stained with May–Grünwald–Giemsa (Merck).

2.7. Iron Quantification in the Bronchoalveolar Lavage Fluid Supernatant

BAL fluid supernatant was concentrated through Speed-Vacuum. Iron measurements were performed using the SFBC kit (Biolabor) following manufacturer's instructions.

2.8. Measurement of Cytokine Protein Levels in Bronchoalveolar Lavage

Cytokine protein levels (IL6, IL1β and TNFα) were determined in BAL fluid supernatants applying Multiplex bead-array based technology. Measurements were performed on a BioPlex200 System using the Bio-Plex Pro Cytokine Reagent Kit and Bio-Plex Pro Mouse Cytokine sets (Bio-Rad) according to manufacturer's instructions. Cytokine protein levels are given as picograms in total BAL fluid supernatant.

2.9. Lung Function Measurements

Mice were anesthetized via intraperitoneal injection of Na^+-pentobarbital (80 mg/kg), tracheostomized and placed on the FlexiVent system (SCIREQ, Montreal, QC, Canada) for measurements of pulmonary function. Mice were then paralyzed with pancuronium bromide injected intraperitoneally (0.8 mg/kg) to avoid breathing artefacts during the measurement. Mice were ventilated at a frequency of 150 breaths/min, with a tidal volume of 11 mL/kg and a positive end expiratory pressure of 3 cm H_2O to prevent alveolar collapse. Pressure-volume curves, total lung capacity, pulmonary compliance and elastance were measured as previously described in (Mall et al., 2008) and (Vanoirbeek et al., 2010). All perturbations were performed until at least three acceptable measurements were reached.

2.10. Blood Oxygen Saturation

Oxygen saturation was determined using a noninvasive pulse oximeter for laboratory animals (MouseOx® Plus, Starr life science) following manufacturer's instructions. Arterial blood oxygen saturation was analyzed in conscious mice exposed to room air with a thigh clip sensor. The oxygen saturation was measured when pulse waves were stable and regular in order to obtain valid values.

2.11. Stereology of Lung Tissue

Lungs from 36 week old mice were instilled via the trachea with 1.5% paraformaldehyde, 1.5% glutaraldehyde in 0.15 M Hepes buffer at hydrostatic pressure of 25 cm and stored in the same solution at 4 °C until further processing. The lungs were embedded in glycol methacrylate according to standard protocol (Muhlfeld et al., 2013) and 1.5 μm thick sections were cut. Light microscopy was performed using a Leica DM6000B microscope (Leica, Wetzlar, Germany) attached to a computer with the newCAST stereology software (Visiopharm, Horsholm, Denmark). Design-based stereology was used to quantify the volume of the lung parenchyma and non-parenchyma as described in (Muhlfeld et al., 2013).

2.12. Erythropoietin (Epo) Measurements

Plasma Epo levels were determined using a mouse Epo ELISA kit (R&D systems) following manufacturer's instructions.

2.13. Isolation and Differentiation of Bone Marrow Derived Macrophages (BMDM)

Bone marrow cells were flushed from tibia and femur using ice-cold Hank's balanced salt solution (HBSS) and filtered through a 70 μm cell strainer (BD biosciences). Cells were seeded at a density of 350,000 cells/cm^2 in RPMI1640-Glutamax medium (Life Technologies) supplemented with 10% of heat-inactivated fetal bovine serum (Hyclone, Thermo scientific), 1% Penicillin/streptomycin (Gibco) and 10 ng/mL M-CSF (Peprotech). After 4 days, non-adherent cells were removed by HBSS washing and the medium was replaced daily until cell harvesting (6 days after seeding). Before harvesting, BMDM were treated overnight with 75 μM of iron-nitrilotriacetate (FeNTA).

2.14. Immunohistochemistry and Immunocytochemistry

Lungs were inflated with 4% neutral buffered formalin (Fischar) to 25 cm of fixative pressure, fixed overnight by immersion in the same solution, dehydrated and paraffin embedded. Lungs were sectioned at 1.5 or 5 μm and mounted on Superfrost Plus slides (ThermoFisher scientific). Lung sections were rehydrated and treated for 10 min with 3% H_2O_2 (Sigma Aldrich) to block endogenous peroxidases. After washing in distilled water, tissue slides were subjected to microwave-mediated antigen retrieval using the Citraplus reagent (Biogenex). After 30 min of cooling, slides were washed 3 times in PBS and subjected to immunorecognition using Vectastain ABC mouse and rabbit kits (Vector Lab, Burlingame, CA, USA) following manufacturer's instructions. BAL cells in cytopsin preparations were fixed in cold acetone (−20 °C) for 10 min, washed in PBS and treated for 10 min with 3% H_2O_2 (Sigma Aldrich) to block endogenous peroxidases. After washing in PBS, cytospin slides were subjected to immunorecognition using the Vectastain ABC rabbit kit (Vector Lab, Burlingame, CA, USA) following manufacturer's instructions. Antibody dilutions and catalog numbers are reported in Supplementary information. Isotype antibodies were used at the same concentration as the primary antibodies to control for antibody specificity. Slides were developed using the Vector AEC substrate (Vector lab), rinsed with distilled water, counterstained with Hematoxylin, washed in PBS and mounted using the VectaMount AQ mounting medium (Vector lab). Images were digitally acquired with a Nikon Ni-E microscope (Nikon Center of the University of Heidelberg), using the Nikon NIS-Elements software. Splenic cells in cytospin preparations were subjected to the same protocol as BAL cells in cytospin preparations and used as a positive control for FPN immunocytochemistry.

2.15. DAB-enhanced Perls' Stain

Lungs were inflated with 4% neutral buffered formalin (Fischar) to 25 cm of fixative pressure, fixed overnight by immersion in the same solution, dehydrated and paraffin embedded. Lungs were sectioned at 1.5 or 5 μm and mounted on Superfrost Plus slides (ThermoFisher scientific). Lung sections were rehydrated and stained for 10 min with a potassium ferrocyanide/HCl solution (Sigma Aldrich). After washing in distilled water, slides were treated with 3,3-diaminobenzidinetetrahydrochloride (DAB) (Sigma Aldrich). Slides were washed again in distilled water, counterstained with Hematoxylin, washed in PBS, dehydrated and mounted using the Eukitt quick-hardening mounting medium (Sigma Aldrich).

2.16. Perls' Stain

BAL cells in cytopsin preparations were stained with potassium ferrocyanide/HCl solution (Sigma Aldrich), washed in distilled water and counterstained with Fast Red (Sigma Aldrich). Images were digitally acquired with a Nikon Ni-E microscope, using the Nikon NIS-Elements Viewer software.

2.17. Hematoxylin and Eosin Stain

Paraffin lung sections were rehydrated and stained for 6 min with Mayer's Hematoxylin (Sigma Aldrich). Slides were washed in water, rinsed in HCl/EtOH, washed again in water and stained for 1 min with Eosin Y (Sigma Aldrich). Slides were dehydrated and mounted using the Entellan new mounting medium (Merck).

2.18. Masson Goldner Trichrome Stain

Paraffin lung sections were rehydrated and stained with Masson Goldner Trichrome Staining Kit (Carl Roth) following manufacturer's instructions.

2.19. Analysis of Lung Collagen Content

Paraffin lung sections (3 μm) were stained with 0.1% Sirius red solution as previously described (Kosanovic et al., 2011). The degree of fibrosis was calculated by the analysis of the total amount of collagen in the left lung (Leica Microsystem, Wetzlar, Germany). For evaluation of the percentage of collagen, the collagen positive areas (red fibers) were determined in a minimum of 300 images per animal.

2.20. Flow Cytometry Analysis

Cells obtained from BAL were stained with CD45.2, CD11c and SiglecF antibodies for 30 min on ice (antibody dilutions and catalog numbers are reported in Supplementary information). To measure oxidative stress, BAL cells and BMDM were incubated for 30 min at RT with 5 μM CellROX Green reagent (ThermoFisher). After washing, cells were analyzed by flow cytometry using the BD LSRFortessa Cell Analyzer.

2.21. Statistical Analyses

Data are shown as mean ± SEM. Statistical analyses were performed using Prism v6 (GraphPad Software, La Jolla, CA). Two-tailed, Student's *t*-test was used and *p*-values < 0.05 (*), <0.01 (**), <0.001 (***) and <0.0001 (****) are indicated.

3. Results

3.1. Iron Levels are Increased in the Lung of Slc40a1^{C326S} Mice

Slc40a1^{C326S} mice, a disease model of HH type 4, is hallmarked by increased systemic iron levels, iron deposition in parenchymal tissues and iron depletion in iron exporting organs (Altamura et al., 2014). We now analyzed lung tissue of male and female heterozygous Slc40a1$^{wt/C326S}$ and homozygous Slc40a1$^{C326S/C326S}$ mice and demonstrate that iron accumulates in an age- and genotype-dependent manner (Fig. 1A).

Under physiological conditions, elevated cellular iron levels inactivate the iron-responsive element/iron-regulatory protein (IRE/IRP) system. This causes degradation of the transcripts encoding for the iron importers divalent metal transporter 1 (DMT1) and transferrin receptor 1 (TfR1) and allows for the translation of the iron storage protein ferritin light chain (FtL) and ferritin heavy chain (FtH) as well as for the iron exporter FPN (Anderson et al., 2012; Muckenthaler et al., 2008). Accordingly, mRNA and protein expression of TfR1 and mRNA expression of the IRE-containing transcript of DMT1 are decreased in iron loaded lungs of Slc40a1$^{wt/C326S}$ and Slc40a1$^{C326S/C326S}$ mice (Fig. 1B, C, D), while FtL protein expression is increased (Fig. 1D). Furthermore, FPN expression shows a genotype-specific increase both at mRNA and protein levels (Fig. 1D, E).

Excess of iron generates reactive oxygen species (ROS) that will damage proteins, lipids and DNA (Altamura and Muckenthaler, 2009; Papanikolaou and Pantopoulos, 2005). Consistently, increased pulmonary iron levels in Slc40a1$^{C326S/C326S}$ mice correlate with increased

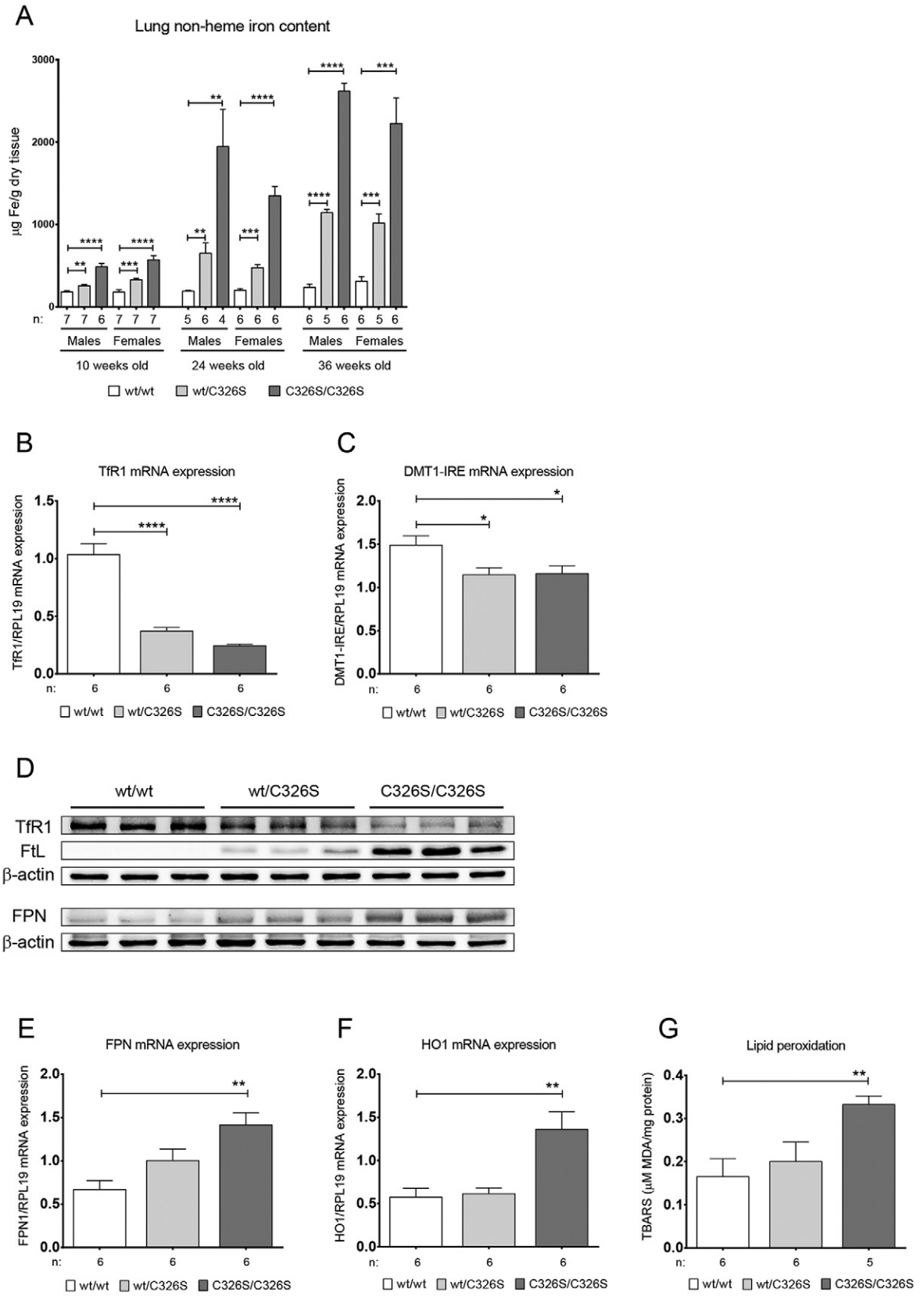

Fig. 1. Slc40a1^{C326S} mice show increased pulmonary iron content. A) Total lung non-heme iron levels measured in male and female 10-, 24- and 36-week old mice. B) qRT-PCR analysis of TfR1 mRNA expression in total lung of female 36-week old mice. C) qRT-PCR analysis of DMT1-IRE mRNA expression in total lung of female 36-week old mice. D) Western Blot analysis of TfR1, FtL and FPN protein expression in total lung of female 36-week old mice. β-actin was used as loading control. E) qRT-PCR analysis of FPN mRNA expression in total lung of female 36-week old mice. F) qRT-PCR analysis of HO1 mRNA expression in total lung of female 36-week old mice. G) Lipid peroxidation measured by the TBARS assay in total lung of female 36-week old mice.

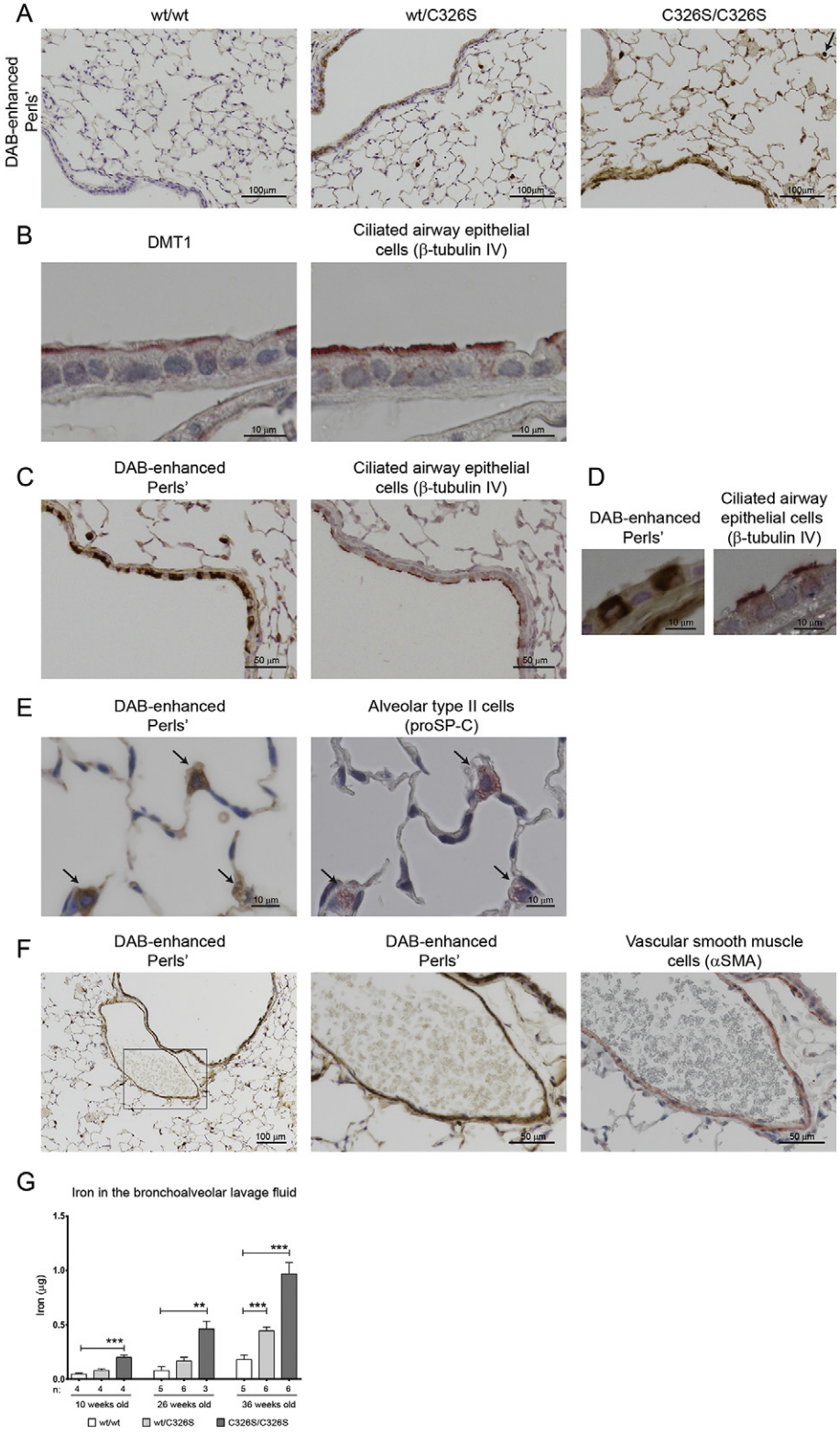

Fig. 2. Iron accumulation in the lung of Slc40a1$^{C326S/C326S}$ mice is restricted to specific cell types. A) DAB-enhanced Perls' staining of lung sections of female 36-week old mice. Arrow shows an alveolar macrophage with strong iron accumulation. B) Immunohistochemistry for DMT1 (left) and β-tubulin IV (right) of consecutive lung sections from wild-type female 36-week old mice. C) DAB-enhanced Perls' staining (left) and immunohistochemistry for β-tubulin IV (right) of consecutive lung sections from Slc40a1$^{C326S/C326S}$ female 26-week old mice. D) Higher magnification of DAB-enhanced Perls' staining (left) and immunohistochemistry for β-tubulin IV (right) of consecutive lung sections from Slc40a1$^{C326S/C326S}$ female 26-week old mice. E) DAB-enhanced Perls' staining (right) and immunohistochemistry against prosurfactant protein C (proSP-C) (left) of consecutive lung sections from Slc40a1$^{C326S/C326S}$ female 36-week old mice. Arrows indicate alveolar type II cells. F) DAB-enhanced Perls' staining (left and center) and immunohistochemistry for alpha smooth muscle actin (αSMA) (right) of consecutive lung sections from Slc40a1$^{C326S/C326S}$ female 36-week old mice. G) Iron levels measured in the bronchoalveolar lavage (BAL) fluid supernatant of 10-, 26- and 36-week old mice.

heme oxygenase 1 (HO-1) mRNA expression, a marker for oxidative stress (Fig. 1F), and with elevated lipid peroxidation (Fig. 1G).

Collectively, our results show that the disruption of the hepcidin/FPN regulatory axis causes iron overload and oxidative stress in the lung.

3.2. Iron Accumulates in Specific Pulmonary Cell Types in Slc40a1^{C326S} Mice

Histological analysis of the lung of Slc40a1^{C326S} mice confirmed the iron overload phenotype and revealed that iron deposition is restricted to specific cell types (Fig. 2A).

Previous reports suggested that airway epithelial cells acquire iron from the airway lumen via DMT1 (Ghio, 2009). In wild-type mice, we detected DMT1 mainly at the apical membrane of ciliated airway epithelial cells (Fig. 2B). In line with this observation, iron was commonly detected in ciliated epithelial cells lining the conducting airways of Slc40a1$^{C326S/C326S}$ mice (Fig. 2C and D). In addition, iron was detected in a subset of another pulmonary epithelial cell type - alveolar type II cells, which line the gas exchanging distal airspaces and produce surfactant proteins such as prosurfactant protein C (Fig. 2E).

Furthermore, vascular smooth muscle cells (SMC) characterized by expression of alpha smooth muscle actin stain for iron (Fig. 2F). Interestingly, vascular SMCs are heterogeneous in regard to iron loading, whereby some show iron overload while others are iron-spared (Fig. S1A). This observation implies that the lung contains at least two populations of vascular SMCs that are hallmarked by differential iron trafficking. Future studies will have to determine whether different populations of vascular SMCs in terms of iron handling may reflect upon their role in maintaining appropriate blood pressure under physiological and/or pathophysiological conditions.

Importantly, increased iron levels were also detected in the bronchoalveolar lavage (BAL) fluid of Slc40a1^{C326S} mice (Fig. 2G).

3.3. Alveolar Macrophages Accumulate Iron in Slc40a1$^{C326S/C326S}$ Mice

Iron accumulation in alveolar macrophages (AM) is a hallmark of certain lung diseases (Ghio et al., 2013; Philippot et al., 2014). Analysis of histological sections of Slc40a1$^{C326S/C326S}$ mice revealed severe iron accumulation in AM (Fig. 2A arrow). We next analyzed the cellular fraction of the BAL by differential May-Grünwald-Giemsa stain and showed that AM were the predominant cell type in the BAL fluid of wild-type and Slc40a1$^{C326S/C326S}$ mice (Fig. 3A, Fig. 3B). Interestingly, the total number of cells in the BAL fluid of Slc40a1$^{C326S/C326S}$ mice was increased, which is explained by an increase in AM (Fig. 3B), a finding confirmed by flow cytometry (Fig. 3C) (Misharin et al., 2013). In both wild-type and Slc40a1$^{C326S/C326S}$ mice, >90% of the immune cells in the BAL fluid correspond to AM (CD45.2^{+} CD11c^{+} SiglecF^{+}) (Fig. 3D). Perls' staining of cytospin preparations revealed severe iron overload in AM of Slc40a1$^{C326S/C326S}$ mice (Fig. 3E). This iron retention phenotype distinguishes AM from hepatic Kupffer cells or splenic reticuloendothelial macrophages in Slc40a1$^{C326S/C326S}$ mice, which are iron depleted (Altamura et al., 2014). It is of note that in the same cell preparations of Slc40a1$^{C326S/C326S}$ mice we also detected iron spared AM (Fig. 3E, arrow), indicating that the population of AM in Slc40a1$^{C326S/C326S}$ mice is heterogeneous regarding iron handling. A heterogeneity in iron accumulation in AM of Slc40a1$^{C326S/C326S}$ mice is possibly explained by a differential expression of FPN (Fig. 3F).

We previously showed that macrophage iron overload results in oxidative stress, which triggers a pro-inflammatory status (Vinchi et al., 2016). We next investigated the degree of oxidative stress in AM as well as the pulmonary inflammatory status in Slc40a1$^{C326S/C326S}$ mice. By applying the CellROX green as ROS reporter, we failed to detect differences in oxidative stress in AM between wild-type and Slc40a1$^{C326S/C326S}$ mice (Fig. S2A). A lack of oxidative stress in iron-loaded AM may be explained by an adaptation to chronic iron accumulation. By contrast, acute iron treatment of bone marrow derived macrophages (BMDM) triggers the formation of oxidative radicals (Fig. S2A). Despite increased numbers of AM in Slc40a1$^{C326S/C326S}$ mice (Fig. 3B), and consistent with a lack of oxidative stress in AM, we failed to detect differences in mRNA and protein levels of inflammatory cytokines (IL1β, IL6 and TNFα) in total lung or in the BAL supernatant, respectively (Fig. S2B, S2C). These observations indicate that increased pulmonary iron levels did not cause pulmonary inflammation in Slc40a1$^{C326S/C326S}$ mice.

3.4. Slc40a1$^{C326S/C326S}$ Mice Show Restrictive Lung Disease and Decreased Blood Oxygen Saturation

Although no differences in lung structure were observed by histological analysis (Fig. S3A-D), we next investigated whether Slc40a1$^{C326S/C326S}$ mice show alterations in lung function. Functional measurements in 36-week old Slc40a1$^{C326S/C326S}$ mice revealed classical signs of restrictive lung disease, such as decreased total lung capacity and decreased lung compliance (Fig. 4A, B). Consistently, Slc40a1$^{C326S/C326S}$ mice show increased pulmonary elastance, thus revealing elevated lung rigidity (Fig. 4C). This observation was confirmed by exposing the mice to fixed air pressures (Flexivent) as shown in the pressure-volume curve (Fig. 4D). We excluded the possibility that the observed differences between wild-type and Slc40a1$^{C326S/C326S}$ mice were due to differences in body size. Despite the fact that aged Slc40a1$^{C326S/C326S}$ mice present with lower body weight most likely due to exocrine pancreatic failure (Altamura et al., 2014), the tibia length, a marker for body size, is comparable to age-matched wild-type mice (Fig. S4A). Furthermore, we detected a decrease in total lung capacity already in 26-week old Slc40a1$^{C326S/C326S}$ mice, which at this age still don't show differences in body weight as well as tibia length (Figs. S4, S5). Stereological analysis of the lung shows that the volume of the lung parenchyma is reduced in Slc40a1$^{C326S/C326S}$ mice, without alterations in the volume of the lung non-parenchyma (Fig. 4E, F). These observations indicate that the decrease in total lung capacity of Slc40a1$^{C326S/C326S}$ mice results from a reduction in the volume of the lung parenchyma.

A major function of the lung is to provide optimal diffusion conditions for efficient oxygen exchange between the atmosphere and the blood stream. Aged Slc40a1$^{C326S/C326S}$ mice show a marked reduction in blood oxygen saturation when compared to wild-type mice (Fig. 4G). Systemic hypoxia is mainly sensed by the kidney which responds by producing the erythroid growth factor, erythropoietin (Epo). Consistent with decreased oxygen saturation, plasma Epo levels are increased in Slc40a1$^{C326S/C326S}$ mice (Fig. 4 H). Increased levels of circulating Epo stimulate erythropoiesis in the bone marrow to restore sufficient oxygen delivery to every cell in the organism. In line with these findings, we observed higher levels of red blood cells, hemoglobin and hematocrit in Slc40a1$^{C326S/C326S}$ mice (Table S1) (Altamura et al., 2014).

4. Discussion

Respiratory diseases are frequently associated with alterations in pulmonary iron homeostasis (Ghio, 2009). Patients with acute respiratory distress syndrome, pulmonary alveolar proteinosis, cystic fibrosis and COPD show higher levels of iron in the lung when compared to healthy individuals (Ghio et al., 2003; Ghio et al., 2012; Ghio et al., 2008; Philippot et al., 2014). So far, the mechanism(s) leading to pulmonary iron accumulation and the role of iron in the development of lung diseases remain unexplored.

Here, we show that the genetic disruption of the regulatory system maintaining systemic iron homeostasis causes age-dependent and genotype-specific pulmonary iron accumulation, increased lipid peroxidation, and gene responses consistent with pulmonary iron overload and oxidative stress; TfR1 and DMT1-IRE expression is decreased and FtL and FPN levels are increased. Elevated FPN protein levels likely result from a combination of transcriptional responses, derepression of FPN

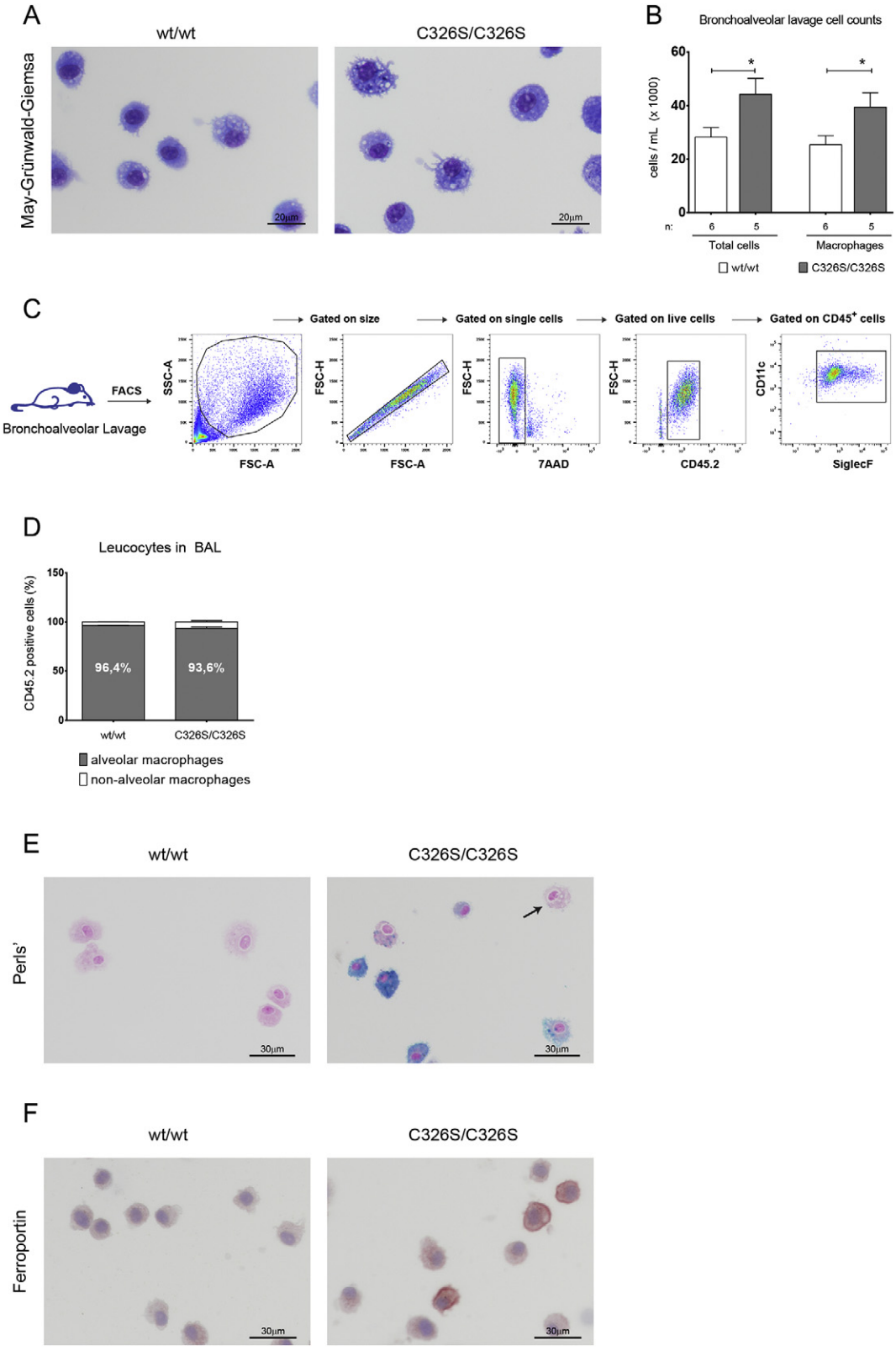

Fig. 3. Alveolar macrophages in Slc40a1$^{C326S/C326S}$ mice show iron deposition. A) May-Grünwald-Giemsa of cytospin preparations of AM obtained from the BAL of male 26-week old mice. B) Total cell count and AM cell count of the BAL fluid of male 26-week old mice. C) Gating strategy used to identify the cells present in the BAL fluid of wild-type and Slc40a1$^{C326S/C326S}$ mice by FACS analysis. D) Percentage of AM (CD11c^{+} SiglecF^{+}) present in the leukocyte fraction (CD45.2^{+}) in the BAL fluid of male 24-week old mice. E) Perls' stain of cytospin preparations of cells isolated from the BAL fluid of male 24-week old mice. Arrow points to an iron spared AM. F) Immunocytochemistry for ferroportin in cytospin preparations of cells isolated from the BAL fluid of male 24-week old mice.

translation via the IRE/IRP system and the hepcidin-resistant phenotype that post-translationally stabilizes the FPN protein (Altamura et al., 2014; Anderson et al., 2012).

Our finding that increased systemic iron levels result in iron accumulation in the lung is supported by a previous study in which intraperitoneal injection of iron-saccharate increased iron levels in the lung

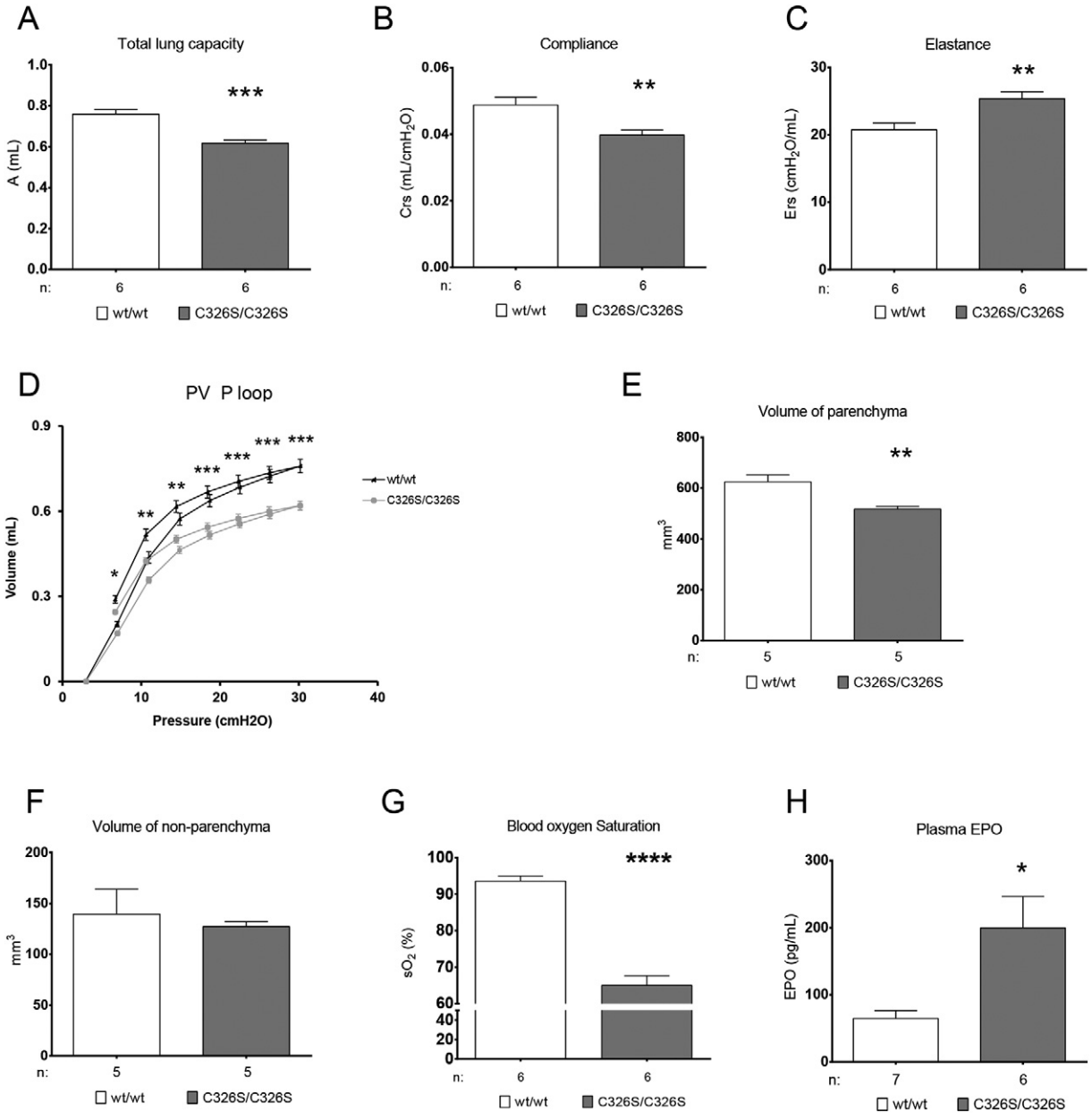

Fig. 4. Impaired lung function and reduced blood oxygen saturation hallmark Slc40a1$^{C326S/C326S}$ mice. (A–D) Lung function measurements performed in female 36-week old mice. A) Total Lung Capacity; B) Dynamic Compliance; C) Elastance; D) Pressure-Volume (PV) curve with controlled pressure applied. E) Volume of lung parenchyma measured in female 36-week old mice. F) Volume of lung non-parenchyma measured in female 36-week old mice. G) Blood oxygen saturation measured in female 36-week old mice. H) Epo levels measured in the plasma of female 36-week old mice.

(Giorgi et al., 2015). While in this study, iron accumulated predominantly in AM, we demonstrate that in addition ciliated airway epithelial cells, alveolar type II cells and vascular SMCs can load iron in Slc40a1$^{C326S/C326S}$ mice. The differences observed in these two mouse models of iron overload may be explained by an acute versus chronic iron overload, by different iron sources or possible local consequences of the disrupted FPN/hepcidin system.

We further show that iron accumulation in Slc40a1$^{C326S/C326S}$ mice does not trigger pulmonary inflammation. However, the availability of free iron in the lung may determine the outcome of pulmonary infections (Khiroya and Turner, 2015). For example, increased pulmonary iron levels are related to the persistence of *Pseudomonas aeruginosa* infection in cystic fibrosis patients (Reid et al., 2007). Moreover, during *Pseudomonas aeruginosa* infection, the murine host up-regulates the expression of proteins involved in iron-sequestration (Damron et al., 2016), highlighting the known competition for iron between the host and the pathogen. Since there is a general increase in pulmonary iron levels in Slc40a1$^{C326S/C326S}$ mice, and in particular in extracellular iron in the bronchoalveolar space, we hypothesize that Slc40a1$^{C326S/C326S}$ mice may have an increased susceptibility to bacterial lung infections. However, this concept needs to be tested experimentally in future studies.

Slc40a1$^{C326S/C326S}$ mice present classical signs of restrictive lung disease, with a decrease in total lung capacity and compliance and an increase in pulmonary elastance. A restrictive pattern is commonly associated with pulmonary fibrosis but collagen deposition in the lung of Slc40a1$^{C326S/C326S}$ mice is not significantly increased and therefore cannot explain the strong phenotype. Rodriguez-Capote and colleagues showed that the presence of ROS and the oxidation of surfactant phospholipids and proteins can alter surfactant function (Rodriguez-Capote et al., 2006). It is thus possible that the presence of extracellular iron in the bronchoalveolar space of Slc40a1$^{C326S/C326S}$ mice may affect

surfactant activity, surface tension and lung compliance. However, the mechanism(s) causing the restrictive pattern in Slc40a1$^{C326S/C326S}$ mice still remain to be elucidated.

It is of note that restrictive lung disease is the predominant pulmonary dysfunction in patients with thalassemia major (Carnelli et al., 2003; Guidotti et al., 2016; Kanj et al., 2000). Due to ineffective erythropoiesis and blood transfusion requirements, these patients present with increased systemic iron levels and parenchymal iron overload. We therefore speculate that the pulmonary restrictive pattern in thalassemia major patients may be a consequence of increased systemic iron levels and/or lung iron deposition (Carnelli et al., 2003; Kanj et al., 2000; Parakh et al., 2007).

Slc40a1$^{C326S/C326S}$ mice show a strong decrease in blood oxygen saturation, despite the absence of observable structural changes in the lung. This finding can be caused by 1) a substantial ventilation/perfusion (V/Q) mismatch, 2) a shunt flow of the blood in Slc40a1$^{C326S/C326S}$ mice or 3) by a low cardiac output. With regard to the first hypothesis, the iron deposition observed in a subset of alveolar type II cells may lead to regional impairment of surfactant production, which may in turn cause a partial collapse of gas exchanging units resulting in ventilation/perfusion mismatch and hypoxemia. Second, a shunting of unoxygenated blood across the heart or the lungs might be caused by abnormal iron deposition in vascular smooth muscle cells leading to the respective vascular dysfunction/abnormalities. Third, low cardiac output could also contribute to such a phenotype by causing low venous O_2 and finally low arterial O_2 saturation. Future studies will be necessary to address these possibilities.

The decrease in blood oxygen saturation correlates with increased plasma EPO levels in Slc40a1$^{C326S/C326S}$ mice. Hypoxia is the main physiological inducer of EPO production in the kidney via the hypoxia inducible factor HIF2α/HIF1β heterodimer (Haase, 2010). In Slc40a1$^{C326S/C326S}$ mice iron may also directly increase HIF-2α mRNA translation by inhibiting the binding of IRPs to its 5′ UTR (Sanchez et al., 2007). Increased plasma levels of EPO stimulate erythropoiesis in the bone marrow. Consistently, we detected high levels of red blood cells, hemoglobin and hematocrit in Slc40a1$^{C326S/C326S}$ mice.

We cannot exclude that pathophysiological consequences of iron overload in Slc40a1$^{C326S/C326S}$ mice other than in the lung may contribute to our observations. The restrictive pattern and decreased blood oxygen saturation may be caused by a combination of high iron levels in the lung as well as other impairments triggered by an increase in systemic iron levels and organ iron deposition (Altamura et al., 2014). To date, there is no evidence of lung pathology in human patients with HH type 4. However, this may reflect upon the fact that patients identified with the FPN C326S point mutation were heterozygous (Sham et al., 2005) and clinical iron overload has been controlled by phlebotomy.

Taken together, our results show that a disruption in the hepcidin/FPN regulatory system leads to an age-dependent pulmonary iron deposition in specific lung cell types. Homozygous Slc40a1$^{C326S/C326S}$ mice show restrictive lung disease and decreased blood oxygen saturation. These observations implicate iron in lung pathology, which so far is not considered a classical iron-related disorder. Moreover, we speculate that an impaired lung function may contribute to the premature death observed in Slc40a1$^{C326S/C326S}$ mice (Altamura et al., 2014).

Funding Sources

This work was supported by research funding from the Dietmar Hopp Stiftung (23011208) (M.U.M.), the German Federal Ministry of Education and Research 82DZL00401 and 82DZL004A1 (M.U.M. and M.A.M), the DFG via the Cluster of Excellence REBIRTH (C.M.), BREATH (C.M.), by a fellowship from Fundação para a Ciência e a Tecnologia, Portugal (SFRH/BD/51702/2011) (J.N.) and by the Deutsche Forschungsgemeinschaft SFB1118 (S.A. and M.U.M.).

Conflict of Interest

The authors declare no conflict of interest.

Author Contributions

J.N. designed the project, performed experiments and wrote the manuscript; D.L. performed the blood oxygen saturation measurements and provided expertise in measurements of lung function; S.K. and N.W. provided expertise in lung physiology and performed analysis of lung collagen content; C.B. and C.M. performed the stereological analysis of the lung; R.A. provided expertise in measurements of lung function and bronchoalveolar lavage analysis; M.A.M. designed and supervised the project; S.A. designed and supervised the project, performed experiments and wrote the manuscript; M.U.M. designed and supervised the project and wrote the manuscript.

Acknowledgements

We thank the EMBL Flow Cytometry facility, in particular Malte Paulsen and Diana Ordonez, for technical assistance. We are grateful to Prof. Dr. Ursula Klingmüller and Dr. Katharina Robichon for support in the Luminex experiment. We thank the personal of the animal facility of the Heidelberg University for the mouse housing and care and the Nikon center at the University of Heidelberg for granting us access to their facility. We thank Katja Müdder for technical assistance.

Appendix A. Supplementary data

Supplementary data to this article can be found online at http://dx.doi.org/10.1016/j.ebiom.2017.04.036.

References

Altamura, S., Muckenthaler, M.U., 2009. Iron toxicity in diseases of aging: Alzheimer's disease, Parkinson's disease and atherosclerosis. J. Alzheimers Dis. 16:879–895. http://dx.doi.org/10.3233/JAD-2009-1010.

Altamura, S., D'Alessio, F., Selle, B., Muckenthaler, M.U., 2010. A novel TMPRSS6 mutation that prevents protease auto-activation causes IRIDA. Biochem. J. 431:363–371. http://dx.doi.org/10.1042/BJ20100668.

Altamura, S., Kessler, R., Grone, H.J., Gretz, N., Hentze, M.W., Galy, B., Muckenthaler, M.U., 2014. Resistance of ferroportin to hepcidin binding causes exocrine pancreatic failure and fatal iron overload. Cell Metab. 20:359–367. http://dx.doi.org/10.1016/j.cmet.2014.07.007.

Anderson, C.P., Shen, M., Eisenstein, R.S., Leibold, E.A., 2012. Mammalian iron metabolism and its control by iron regulatory proteins. Biochim. Biophys. Acta 1823:1468–1483. http://dx.doi.org/10.1016/j.bbamcr.2012.05.010.

Carnelli, V., D'Angelo, E., Pecchiari, M., Ligorio, M., D'Angelo, E., 2003. Pulmonary dysfunction in transfusion-dependent patients with thalassemia major. Am. J. Respir. Crit. Care Med. 168:180–184. http://dx.doi.org/10.1164/rccm.200211-1292OC.

Damron, F.H., Oglesby-Sherrouse, A.G., Wilks, A., Barbier, M., 2016. Dual-seq transcriptomics reveals the battle for iron during Pseudomonas aeruginosa acute murine pneumonia. Sci. Rep. 6:39172. http://dx.doi.org/10.1038/srep39172.

Galy, B., Ferring, D., Benesova, M., Benes, V., Hentze, M.W., 2004. Targeted mutagenesis of the murine IRP1 and IRP2 genes reveals context-dependent RNA processing differences in vivo. RNA 10:1019–1025. http://dx.doi.org/10.1261/rna.7220704.

Ghio, A.J., 2009. Disruption of iron homeostasis and lung disease. Biochim. Biophys. Acta 1790:731–739. http://dx.doi.org/10.1016/j.bbagen.2008.11.004.

Ghio, A.J., Carter, J.D., Richards, J.H., Brighton, L.E., Lay, J.C., Devlin, R.B., 1998. Disruption of normal iron homeostasis after bronchial instillation of an iron-containing particle. Am. J. Physiol. 274, L396–L403.

Ghio, A.J., Carter, J.D., Richards, J.H., Richer, L.D., Grissom, C.K., Elstad, M.R., 2003. Iron and iron-related proteins in the lower respiratory tract of patients with acute respiratory distress syndrome. Crit. Care Med. 31:395–400. http://dx.doi.org/10.1097/01.CCM.0000050284.35609.97.

Ghio, A.J., Stonehuerner, J.G., Richards, J.H., Crissman, K.M., Roggli, V.L., Piantadosi, C.A., Carraway, M.S., 2008. Iron homeostasis and oxidative stress in idiopathic pulmonary alveolar proteinosis: a case-control study. Respir. Res. 9:10. http://dx.doi.org/10.1186/1465-9921-9-10.

Ghio, A.J., Roggli, V.L., Soukup, J.M., Richards, J.H., Randell, S.H., Muhlebach, M.S., 2012. Iron accumulates in the lavage and explanted lungs of cystic fibrosis patients. J. Cyst. Fibros. 12:390–398. http://dx.doi.org/10.1016/j.jcf.2012.10.010.

Ghio, A.J., Roggli, V.L., Soukup, J.M., Richards, J.H., Randell, S.H., Muhlebach, M.S., 2013. Iron accumulates in the lavage and explanted lungs of cystic fibrosis patients. J. Cyst. Fibros. 12:390–398. http://dx.doi.org/10.1016/j.jcf.2012.10.010.

Giorgi, G., Danna, M.C., Roque, M.E., 2015. Iron homeostasis and its disruption in mouse lung in iron deficiency and overload. Exp. Physiol. http://dx.doi.org/10.1113/EP085166.

Guidotti, F., Piatti, G., Marcon, A., Cassinerio, E., Giuditta, M., Roghi, A., Fasano, V., Consonni, D., Cappellini, M.D., 2016. Pulmonary dysfunction in thalassaemia major: is there any relationship with body iron stores? Br. J. Haematol. http://dx.doi.org/10.1111/bjh.14396.

Haase, V.H., 2010. Hypoxic regulation of erythropoiesis and iron metabolism. Am. J. Physiol. Ren. Physiol. 299:F1–13. http://dx.doi.org/10.1152/ajprenal.00174.2010.

Kanj, N., Shamseddine, A., Gharzeddine, W., Kanj, M., Nasr, T.A., Koussa, S., Jibrail, J., Taher, A., 2000. Relation of ferritin levels to pulmonary function in patients with thalassemia major and the acute effects of transfusion. Eur. J. Haematol. 64:396–400. http://dx.doi.org/10.1034/j.1600-0609.2000.90106.x.

Khiroya, H., Turner, A.M., 2015. The role of iron in pulmonary pathology. Multidiscip. Respir. Med. 10:34. http://dx.doi.org/10.1186/s40248-015-0031-2.

Kosanovic, D., Kojonazarov, B., Luitel, H., Dahal, B.K., Sydykov, A., Cornitescu, T., Janssen, W., Brandes, R.P., Davie, N., Ghofrani, H.A., et al., 2011. Therapeutic efficacy of TBC3711 in monocrotaline-induced pulmonary hypertension. Respir. Res. 12:87. http://dx.doi.org/10.1186/1465-9921-12-87.

Livak, K.J., Schmittgen, T.D., 2001. Analysis of relative gene expression data using real-time quantitative PCR and the 2(-Delta Delta C(T)) method. Methods 25:402–408. http://dx.doi.org/10.1006/meth.2001.1262.

Mall, M.A., Harkema, J.R., Trojanek, J.B., Treis, D., Livraghi, A., Schubert, S., Zhou, Z., Kreda, S.M., Tilley, S.L., Hudson, E.J., et al., 2008. Development of chronic bronchitis and emphysema in beta-epithelial Na+ channel-overexpressing mice. Am. J. Respir. Crit. Care Med. 177:730–742. http://dx.doi.org/10.1164/rccm.200708-1233OC.

Misharin, A.V., Morales-Nebreda, L., Mutlu, G.M., Budinger, G.R., Perlman, H., 2013. Flow cytometric analysis of macrophages and dendritic cell subsets in the mouse lung. Am. J. Respir. Cell Mol. Biol. 49:503–510. http://dx.doi.org/10.1165/rcmb.2013-0086MA.

Muckenthaler, M.U., Galy, B., Hentze, M.W., 2008. Systemic iron homeostasis and the iron-responsive element/iron-regulatory protein (IRE/IRP) regulatory network. Annu. Rev. Nutr. 28:197–213. http://dx.doi.org/10.1146/annurev.nutr.28.061807.155521.

Muckenthaler, M.U., Rivella, S., Hentze, M.W., Galy, B., 2017. A red carpet for iron metabolism. Cell 168:344–361. http://dx.doi.org/10.1016/j.cell.2016.12.034.

Muhlfeld, C., Knudsen, L., Ochs, M., 2013. Stereology and morphometry of lung tissue. Methods Mol. Biol. 931:367–390. http://dx.doi.org/10.1007/978-1-62703-056-4_18.

Nemeth, E., Tuttle, M.S., Powelson, J., Vaughn, M.B., Donovan, A., Ward, D.M., Ganz, T., Kaplan, J., 2004. Hepcidin regulates cellular iron efflux by binding to ferroportin and inducing its internalization. Science 306:2090–2093. http://dx.doi.org/10.1126/science.1104742.

Papanikolaou, G., Pantopoulos, K., 2005. Iron metabolism and toxicity. Toxicol. Appl. Pharmacol. 202:199–211. http://dx.doi.org/10.1016/j.taap.2004.06.021.

Parakh, A., Dubey, A.P., Chowdhury, V., Sethi, G.R., Jain, S., Hira, H.S., 2007. Study of pulmonary function tests in thalassemic children. J. Pediatr. Hematol. Oncol. 29:151–155. http://dx.doi.org/10.1097/MPH.0b013e318033a73d.

Philippot, Q., Deslee, G., Adair-Kirk, T.L., Woods, J.C., Byers, D., Conradi, S., Dury, S., Perotin, J.M., Lebargy, F., Cassan, C., et al., 2014. Increased iron sequestration in alveolar macrophages in chronic obstructive pulmonary disease. PLoS One 9, e96285. http://dx.doi.org/10.1371/journal.pone.0096285.

Qiao, B., Sugianto, P., Fung, E., Del-Castillo-Rueda, A., Moran-Jimenez, M.J., Ganz, T., Nemeth, E., 2012. Hepcidin-induced endocytosis of ferroportin is dependent on ferroportin ubiquitination. Cell Metab. 15:918–924. http://dx.doi.org/10.1016/j.cmet.2012.03.018.

Reid, D.W., Carroll, V., O'May, C., Champion, A., Kirov, S.M., 2007. Increased airway iron as a potential factor in the persistence of Pseudomonas aeruginosa infection in cystic fibrosis. Eur. Respir. J. 30:286–292. http://dx.doi.org/10.1183/09031936.00154006.

Rodriguez-Capote, K., Manzanares, D., Haines, T., Possmayer, F., 2006. Reactive oxygen species inactivation of surfactant involves structural and functional alterations to surfactant proteins SP-B and SP-C. Biophys. J. 90:2808–2821. http://dx.doi.org/10.1529/biophysj.105.073106.

Sanchez, M., Galy, B., Muckenthaler, M.U., Hentze, M.W., 2007. Iron-regulatory proteins limit hypoxia-inducible factor-2alpha expression in iron deficiency. Nat. Struct. Mol. Biol. 14:420–426. http://dx.doi.org/10.1038/nsmb1222.

Sham, R.L., Phatak, P.D., West, C., Lee, P., Andrews, C., Beutler, E., 2005. Autosomal dominant hereditary hemochromatosis associated with a novel ferroportin mutation and unique clinical features. Blood Cells Mol. Dis. 34:157–161. http://dx.doi.org/10.1016/j.bcmd.2004.12.002.

Sham, R.L., Phatak, P.D., Nemeth, E., Ganz, T., 2009. Hereditary hemochromatosis due to resistance to hepcidin: high hepcidin concentrations in a family with C326S ferroportin mutation. Blood 114:493–494. http://dx.doi.org/10.1182/blood-2009-04-216226.

Torrance, J.D., Bothwell, T.H., 1968. A simple technique for measuring storage iron concentrations in formalinised liver samples. South Afr. J. Med. Sci. 33, 9–11.

Vanoirbeek, J.A., Rinaldi, M., De Vooght, V., Haenen, S., Bobic, S., Gayan-Ramirez, G., Hoet, P.H., Verbeken, E., Decramer, M., Nemery, B., et al., 2010. Noninvasive and invasive pulmonary function in mouse models of obstructive and restrictive respiratory diseases. Am. J. Respir. Cell Mol. Biol. 42:96–104. http://dx.doi.org/10.1165/rcmb.2008-0487OC.

Vinchi, F., Costa da Silva, M., Ingoglia, G., Petrillo, S., Brinkman, N., Zuercher, A., Cerwenka, A., Tolosano, E., Muckenthaler, M.U., 2016. Hemopexin therapy reverts heme-induced proinflammatory phenotypic switching of macrophages in a mouse model of sickle cell disease. Blood 127:473–486. http://dx.doi.org/10.1182/blood-2015-08-663245.

Wang, X., Ghio, A.J., Yang, F., Dolan, K.G., Garrick, M.D., Piantadosi, C.A., 2002. Iron uptake and Nramp2/DMT1/DCT1 in human bronchial epithelial cells. Am. J. Phys. Lung Cell. Mol. Phys. 282:L987–L995. http://dx.doi.org/10.1152/ajplung.00253.2001.